Time-dependent Schrödinger equation solver for atomic and diatomic systems

Yonas Gebre

July 2023

1 Introduction

The provided documentation presents a code designed to study ultrafast physics, focusing on electron dynamics in atoms, molecules, and materials at the attosecond scale. The code models the use of ultrashort laser pulses to investigate various fascinating ultrafast phenomena by manipulating laser polarization and pulse combinations. This project aims to develop a numerical solution for the time-dependent Schrödinger equation (TDSE) that explores the interaction between atoms, diatomic systems, and intense laser pulses. This documentation comprehensively outlines the code's functionalities, usage instructions, as well as the mathematical and physical principles underlying the modeling of light-matter interaction.

2 acknowledgements

This project was done with work funded by the National Science Foundation (NSF) and the U.S. Department of Energy. It was conducted under the guidance of Andreas Becker, a research professor at JILA, University of Colorado Boulder. Joel Venzke, a former graduate student, made significant contributions to this endeavor.

3 How to use the code

This section will soon be updated to make it less dependent on non-standard libraries. Modifications are being made to enhance compatibility with commonly used libraries, resulting in a more streamlined and accessible approach.

4 Description of the numerical method implemented in the code

[1]

The interaction of atomic systems with electromagnetic fields can be described using the time-dependent Schrödinger equation (TDSE). The TDSE is given by

$$\begin{aligned} i\frac{\partial}{\partial t}\Psi &= \hat{H}\Psi \\ \hat{H} &= \hat{H}_o + V_{int} \end{aligned} \tag{1}$$

where Ψ is the wave function, $\hat{H}$ is the Hamiltonian of the system and i is the imaginary number. The Hamiltonian consists of the atomic system Hamiltonian ($\hat{H}_o$) and the interaction potential (V_{int}). The atomic system Hamiltonian for a system of N_e electrons and N_n fixed nuclei can be written as

$$\hat{H}_o = \sum_{i=1}^{N_e}\left(\frac{\hat{\mathbf{p}}_i^{\,2}}{2} - \sum_{n=1}^{N_n}\frac{Z_n}{r_{i,n}}\right) + \sum_{e_1<e_2}^{N_e}\frac{1}{r_{e_1,e_2}}, \tag{2}$$

where $\hat{\mathbf{p}}_i$ is the momentum operator of the i^{th} electron and Z_n is the charge of the n^{th} nucleus. The r_{e_i,e_j} term corresponds to the distance between the i^{th} and j^{th} electron, and $r_{i,n}$ is the distance between the i^{th} electron and the n^{th} nuclei. The interaction potential term of the Hamiltonian represents the interaction of the atomic system with the laser pulse. The interaction term will be discussed in the next section where we make some approximations to obtain the form that we use in our work. There are currently no known analytical solutions for the TDSE that works for the laser parameters used in our work. Instead, we use numerical solutions to solve the TDSE and to study electron dynamics driven by the laser fields. Due to the large-scale computation necessary for numerical solutions, the TDSE can only be solved numerically for systems with at most two active electrons. In most cases, we focus on processes that can be modeled by simulating the dynamics of a single active electron and assuming a mean-field approach for the rest of the system. In the next section, we present the methodology behind our approach and the approximations used to implement a numerical solver of the TDSE.

[1] This section was also published in my Thesis which can be found in the JILA/University of Colorado Physics department website.

5 Approximations

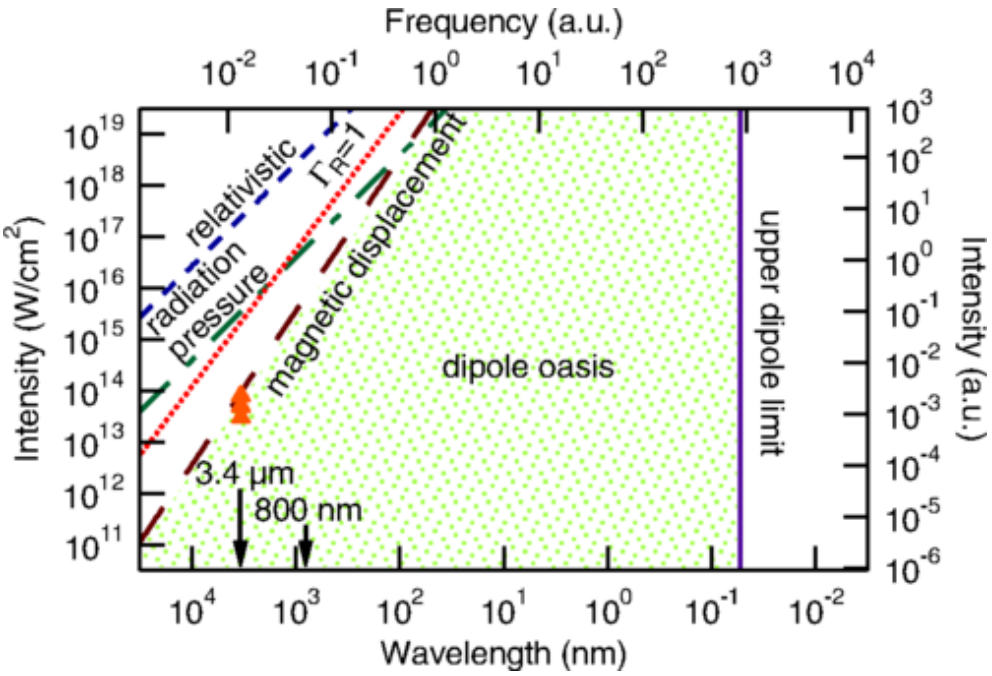

Figure 1: Regions of laser parameters where the dipole and non-relativistic approximations are valid (taken from [**?**]).

To find a numerical solution of the TDSE we make some approximations. The first one is to treat the electromagnetic field classically using Maxwell's equations. This approximation holds for laser pulses with high intensity or large numbers of photons. For the intensities used in our work ($10^{13} - 10^{14}$ W/cm^2), this approximation holds. Second, we use the dipole and non-relativistic approximation [**?**]. In this approximation, we neglect the spatial variation of the laser pulse and assume that it is uniform across the size of the atom. This assumption is valid when the wavelength of the laser pulse is much larger than the radius of the atom, i.e. $\lambda \gg r_{atom}$. We also neglect the magnetic component of the field as it has a negligible contribution to the interaction for the laser parameters used in our study. The parameter space for the laser field where these approximations are valid is referred to as the dipole oasis and is shown in Fig. 1.

With the dipole and non-relativistic approximation and a semi-classical treatment of the laser pulse, the laser interaction term of the Hamiltonian can

be written as (either in length or in velocity gauge):

$$\begin{aligned} V_{int} &= \sum_i -\mathbf{E}(t) \cdot \mathbf{r_i} \\ V_{int} &= \sum_i -\hat{\mathbf{p}}_\mathbf{i} \cdot \mathbf{A}(t), \end{aligned} \tag{3}$$

where $\mathbf{E}$ and $\mathbf{A}$ are the electric field and vector potential of the laser field, respectively. To model systems other than the hydrogen atom, an effective potential must be used. An effective potential is necessary to include the (static) effects of other electrons in our model without solving the TDSE directly for more than one electron. We include the effects of other electrons by using the single active electron approximation (SAE). In the SAE approximation, all electrons except one are considered to be static or frozen in place. The laser is assumed to only interact with the 'active' electron and the dynamics of that electron are studied. With the SAE approximation, the TDSE can is written as

$$i\frac{\partial}{\partial t}\psi(\mathbf{r},t) = \left[-\frac{1}{2}\nabla^2 + V_{SAE}(\mathbf{r}) + V_{int}(\mathbf{r},t)\right]\psi(\mathbf{r},t) \tag{4}$$

where ψ is the wave function of the active electron and V_{int} is the interaction term described in Eqn.3 for a single electron. The SAE potential is given by

$$V_{SAE}\ (r) = \frac{-Z}{r} - \frac{-Z_c e^{-cr}}{r} - \sum_n a_n e^{-b_n r}. \tag{5}$$

The constants a_n, b_n, and c are fit parameters. The SAE potentials in Eq. 5 are determined by fitting the functional form to a potential obtained from density functional theory (DFT) [**?**]. The TDSE equation 4 is used to model all the laser-atom interactions that we consider in this study.

6 Ab-initio solution

Ab-initio methods are ones that solve the TDSE directly from first principles. As mentioned above the TDSE does not have an analytical solution and some approximations are made to solve it numerically. In the ab-initio approach, only a simple system with one, at most two active electrons can be solved. In this work, only systems with one active electron will be studied. Here the ab-initio method used to solve the TDSE for all the calculations in our study is outlined.

6.1 Basis and coordinate system

Our numerical solution uses a finite difference method to represent the wave function on a grid in a three-dimensional coordinate system. To exploit the spherical symmetry of the potential in Eq. 5, spherical coordinates (r, ϕ, θ) are

used to represent the wave function. In this coordinate system, we look for a separable solution for the wave function and choose the following basis

$$\psi(\mathbf{r},t) = \sum_{lm} \frac{\chi_l(r)}{r} Y_{lm}(\theta,\phi) = \sum_{lm} |lm\rangle\,, \tag{6}$$

where $\chi_l(r)$ denotes the radial portion of the wave function, $Y_{lm}(\theta,\phi)$ corresponds to the spherical harmonics, and l, and m represent the orbital, and magnetic quantum numbers, respectively. We express the radial component on a grid, while the angular components are expressed using a spherical harmonic basis. The operators in the Hamiltonian are represented by matrices in our chosen basis, and the matrix elements are computed by evaluating the inner product as

$$H_{lml'm'} = \langle lm|\, H\, |l'm\rangle\,. \tag{7}$$

Since the radial portion is represented on a grid, the integral above is done over the solid angle. The spatial derivatives in the Hamiltonian can be represented using the finite difference method. The first and second-order derivatives in the Hamiltonian can be discretized on the grid as

$$\frac{d}{dx} f(x) \approx \frac{f(x-2h) - 8f(x-h) + 8f(x+h) - f(x+2h)}{12h} \tag{8}$$

$$\frac{d^2}{dx^2} f(x) \approx \frac{-f(x-2h) + 16f(x-h) - 30f(x) + 16f(x+h) - f(x+2h)}{12h^2}. \tag{9}$$

The accuracy of the method can be calculated using Taylor expansion of the finite element terms with respect to $f(x)$. For the central difference formula that is shown in Eqns 8 and 9, the accuracy is the grid spacing to the fourth power or $O(h^4)$. In the upcoming sections, we will compute the matrix elements for each term in the Hamiltonian. The procedure involves obtaining an expression for the operators in spherical coordinates and then evaluating the inner product with our chosen basis.

6.2 Kinetic energy

The kinetic energy term in the Hamiltonian is the Laplace operator scaled by a constant, which can be written in spherical coordinates as

$$T = -\frac{\nabla^2}{2} = -\frac{1}{2r^2}\left[r\frac{\partial^2}{\partial r^2} r + \frac{1}{\sin(\theta)}\frac{\partial}{\partial\theta}\left(\sin(\theta)\frac{\partial}{\partial\theta}\right) + \frac{1}{\sin^2(\theta)}\frac{\partial^2}{\partial\phi^2}\right]. \tag{10}$$

The angular part of the kinetic energy term is the angular momentum operator $\mathbf{L}$ and we can write Eq. 10 as

$$T = \frac{1}{2r}\frac{\partial^2}{\partial r^2} r - \frac{\mathbf{L}^2}{2r^2}. \tag{11}$$

Spherical harmonics are used to expand our wave function which are eigenvectors of the angular momentum operator. When $\mathbf{L}$ acts on the basis we get the following well-known eigenvalues

$$\mathbf{L}^2 \left| l'm' \right\rangle = l'(l'+1) \left| l'm' \right\rangle . \tag{12}$$

Using Eqns 11 and 12 the matrix element for the kinetic energy operator is given by

$$T_{lml'm'} = \left\langle lm \left| \frac{\nabla^2}{2} \right| l'm' \right\rangle = \left\langle lm \left| \frac{1}{2r} \frac{\partial^2}{\partial r^2} r - \frac{l'(l'+1)}{2r^2} \right| l'm' \right\rangle \tag{13}$$

$$T_{lml'm'} = \int \frac{\chi_l(r)}{r} Y^*_{lm} \left(\frac{1}{2r} \frac{\partial^2}{\partial r^2} r - \frac{l'(l'+1)}{2r^2} \right) \frac{\chi_{l'}(r)}{r} Y_{l'm'} d\Omega. \tag{14}$$

Using the orthogonality of the spherical harmonics, Eq. 14 simplifies to

$$T_{lml'm'} = \delta_{ll'mm'} \frac{\chi_l(r)}{r} \left(\frac{1}{2} \frac{d^2}{dr^2} - \frac{l'(l'+1)}{2r^2} \right) \frac{\chi_{l'}(r)}{r}, \tag{15}$$

where the derivative will be represented on the grid using the finite difference discretization scheme, as discussed in section 6.1. The matrix has a tri-diagonal and five-diagonal structure respectively for second and fourth-order finite difference representation of the derivative.

6.3 Single active electron potential

The matrix element for the SAE potential given by Eq. 5 is much simpler since the single-active electron potential used in the present work has spherical symmetry. The matrix elements for the SAE potential is given by

$$V_{lml'm'} = \left\langle lm \left| -\frac{Z}{r} - \frac{Z_c e^{-cr}}{r} - \sum_n a_n e^{-b_n r} \right| l'm' \right\rangle . \tag{16}$$

As before we use the orthogonality of the spherical harmonics and Eq. 16 simplifies to

$$V_{lml'm'} = \delta_{ll'mm'} \frac{\chi_l(r)}{r} \left(-\frac{z}{r} - \frac{Z_c e^{-cr}}{r} - \sum_n a_n e^{-b_n r} \right) \frac{\chi_{l'}(r)}{r}. \tag{17}$$

6.4 Laser coupling in length gauge

The laser coupling term in length gauge in the dipole and non-relativistic approximation is written as

$$V_{int}(\mathbf{r}, t) = -\mathbf{E}(\mathbf{t}) \cdot \mathbf{r}. \tag{18}$$

The matrix elements are more easily calculated if we use a Cartesian coordinate system to expand the dot product and then convert it back to spherical coordinates when taking the inner product with our basis. When expanding the dot product we have

$$V_{int}(\mathbf{r},t) = -E_z z - E_x x - E_y y, \tag{19}$$

where E_i is the electric field in the i-th coordinate. Eq. 19 can be expressed in spherical coordinates using the Cartesian expansion of the spherical harmonics given by

$$\begin{aligned} z &= \sqrt{\frac{4\pi}{3}} r Y_{00}(\theta,\phi) \\ y &= i\sqrt{\frac{2\pi}{3}} r \left(Y_{1-1}(\theta,\phi) + Y_{11}(\theta,\phi)\right) \\ x &= \sqrt{\frac{2\pi}{3}} r \left(Y_{1-1}(\theta,\phi) - Y_{11}(\theta,\phi)\right). \end{aligned} \tag{20}$$

Using Eqns 20 we can calculate the matrix elements of the laser coupling term for each axis of polarization. For polarization in the z-axis, the matrix elements are

$$\begin{aligned} D_{lml'm'} &= \left\langle lm \left| -E_z \sqrt{\frac{4\pi}{3}} r Y_{00} \right| l'm' \right\rangle \\ D_{lml'm'} &= -E_z \sqrt{\frac{4\pi}{3}} \int_S Y_{lm} Y_{00} Y_{l'm'}\, d\Omega \left(\frac{\chi_l(r)}{r} r \ \frac{\chi_{l'}(r)}{r} \right). \end{aligned} \tag{21}$$

This can be simplified further by noting that the integral of three spherical harmonics can be written in terms of the Clebsch-Gordan coefficient as

$$\int_{4\pi} Y^*_{l_1 m_1} Y^*_{l_2 m_2} Y_{l_3 m_3} = (-1)^{m_1} \sqrt{\frac{(2l_1+1)(2l_2+1)}{4\pi(2l_3+1)}} \langle l_1, 0, l_2, 0 | l_3, 0\rangle \langle l_1, m_1, l_2, m_2 | l_3, m_3\rangle. \tag{22}$$

When applying Eq. 22 to our expression, the matrix element for the laser coupling with a laser field polarized along the z-axis can be written as

$$D_{lml'm'} = -E_z (-1)^m \sqrt{\frac{(2l+1)(2l'+1)}{12\pi}} \langle l, 0, 1, 0 | l', 0\rangle \langle l', -m, 1, 0 | l', m'\rangle \left(\frac{\chi_l(r)}{r} r \ \frac{\chi_{l'}(r)}{r} \right). \tag{23}$$

The same procedure can be used to calculate the laser coupling term for fields polarized in the x-axis and y-axis. Using Eqns 20 and 22 the matrix elements for x-axis polarization are given by

$$\begin{aligned} D_{lml'm'} = -E_x (-1)^m \sqrt{\frac{(2l+1)(2l'+1)}{12\pi}} \langle l, 0, 1, 0 | l', 0\rangle \times \\ \left(\langle l', -m, 1, -1 | l', m'\rangle - \langle l', -m, 1, 1 | l', m'\rangle \right) \left(\frac{\chi_l(r)}{r} r \ \frac{\chi_{l'}(r)}{r} \right). \end{aligned} \tag{24}$$

Similarly for y-axis polarization we get

$$D_{lml'm'} = -iE_y(-1)^m \sqrt{\frac{(2l+1)(2l'+1)}{12\pi}} \langle l,0,1,0|l',0\rangle \times \\ \left(\langle l',-m,1,-1|l',m'\rangle + \langle l',-m,1,1|l',m'\rangle\right) \begin{pmatrix} \frac{\chi_l(r)}{r} r & \frac{\chi_{l'}(r)}{r} \end{pmatrix} \\ . \tag{25}$$

The matrix elements show how different angular momentum states are coupled to each other. The coupling determines the transitions between states that are allowed in our system. This is commonly referred to as the selection rules. We can get the selection rules for the system by using the properties of the Clebsch-Gordan coefficients. For fields polarized in the z-axis, the condition $m = m'$ and $|l' - l| = 1$ must be satisfied to have a non-zero matrix element. For light polarized in the x- and y-axis, the selection rules are $|m' - m| = 1$ and $|l' - l| = 1$. The selection rules allow us to know the elements of the laser coupling matrix that are zero, eliminating the need to compute those. This greatly reduces the amount of computation needed when using ab-initio calculations.

6.5 Laser coupling in velocity gauge

The laser coupling term in velocity gauge within the dipole and non-relativistic approximation is given by

$$D(r,t) = -\hat{\mathbf{p}} \cdot \mathbf{A}(t). \tag{26}$$

In Cartesian coordinates, this can be expressed as

$$D(r,t) = iA_x \frac{\partial}{\partial x} + iA_y \frac{\partial}{\partial y} + iA_z \frac{\partial}{\partial z}. \tag{27}$$

The calculation for the matrix elements can be simplified by expressing the laser coupling operator in terms of other operators that have simple matrix elements. We do this by using the commutation relations for the momentum operator given by

$$\hat{p_i} = [\nabla^2, r_i]. \tag{28}$$

The commutation relation allows us to express the laser coupling in terms of the Laplace and position operator. We have calculated the matrix elements for the Laplace and position operator in section 6.2 and 6.4 respectively and the results are used here. For a field linearly polarized in the z-axis the matrix elements can be calculated as follows:

$$D(r,t) = iA_z \frac{\partial}{\partial z} = iA_z[\nabla^2, z] \tag{29}$$

$$D_{lml'm'} = \left\langle lm \left| iA_z \frac{\partial}{\partial z} \right| l'm' \right\rangle \tag{30}$$

$$D_{lml'm'} = \left\langle lm \left| iA_z[\nabla^2, z] \right| l'm' \right\rangle . \tag{31}$$

We can now take the inner product to calculate the matrix elements in our basis. Using the results from sections 6.2 and 6.4 we have

$$D_{lml'm'} = iA_z 2\sqrt{\frac{4\pi}{3}} \left\langle lm \left| Y_{10}(\theta,\phi)\frac{\partial}{\partial r} + \frac{-\mathbf{L}^2 Y_{10}(\theta,\phi) + Y_{10}(\theta,\phi)\mathbf{L}^2}{2r} \right| l'm' \right\rangle \tag{32}$$

$$D_{lml'm'} = iA_z 2 \left\langle lm \left| \frac{\partial}{\partial r} + \frac{-l'(l'+1)+l(l+1)}{2r} \right| l'm' \right\rangle . \tag{33}$$

$$D_{lml'm'} = iA_z 2(-1)^m \sqrt{\frac{(2l+1)(2l'+1)}{12\pi}} \langle l,0,1,0|l',0\rangle \langle l',-m,1,0|l',m'\rangle \times \chi_l(r)\left(\frac{\partial}{\partial r} + \frac{-l'(l'+1)+l(l+1)}{2r}\right)\chi_{l'}(r), \tag{34}$$

The matrix elements for the other two polarization axes are calculated using the same procedure. Here we simply state the results. The matrix elements for x-axis polarization are given by

$$D_{lml'm'} = iA_x 2(-1)^m \sqrt{\frac{(2l+1)(2l'+1)}{12\pi}} \langle l,0,1,0|l',0\rangle \left(\langle l',-m,-1,0|l',m'\rangle - \langle l',-m,1,0|l',m'\rangle\right)\chi_l(r)\left(\frac{\partial}{\partial r} + \frac{-l'(l'+1)+l(l+1)}{2r}\right)\chi_{l'}(r) \tag{35}$$

and for y-axis polarization the matrix elements are

$$D_{lml'm'} = iA_y 2(-1)^m \sqrt{\frac{(2l+1)(2l'+1)}{12\pi}} \langle l,0,1,0|l',0\rangle \left(\langle l',-m,-1,0|l',m'\rangle + \langle l',-m,1,0|l',m'\rangle\right)\chi_l(r)\left(\frac{\partial}{\partial r} + \frac{-l'(l'+1)+l(l+1)}{2r}\right)\chi_{l'}(r) \tag{36}$$

The first order derivative in the velocity gauge laser coupling term is represented using finite difference as explained in section 6.1. As anticipated due to the gauge invariance of the TDSE, the Clebsch-Gordan coefficients reveal that the selection rules for both the length gauge and the velocity gauge are identical. It is important to note that while the ab-initio method explained here maintains gauge invariance, the numerical properties of the method differ depending on the interaction Hamiltonian employed to represent the atom-laser coupling. For a converged result all calculations of the observables are the same irrespective of the gauge. However, the velocity gauge exhibits faster convergence when considering the expansion required in spherical harmonics. This discrepancy is

attributed to the canonical momentum of the Hamiltonian, which is expressed differently for the length and velocity gauges. The canonical momentum is given by

$$\begin{aligned} \Pi &= m\dot{\mathbf{r}} \quad \text{for length gauge and} \\ \Pi &= m\dot{\mathbf{r}} - q\mathbf{A} \quad \text{for velocity gauge} \end{aligned} \tag{37}$$

In the velocity gauge, the electron's canonical momentum incorporates the momentum gained from the laser field and subtracts it from the kinetic energy momentum component. As a result, the momentum in the velocity gauge is typically much smaller compared to the length gauge. This difference leads to the requirement of fewer terms in the expansion in the velocity gauge, as the degree of the spherical harmonics is linked to the electron's momentum.

6.6 Bound and continuum states

The states of any atomic (or other) system can be distinguished into bound and continuum states. Bound states have energies that are discrete and negative while continuum states have energies that are positive and form a continuous spectrum. The states correspond to the eigenstates of the field-free Hamiltonian ($\hat{H}_o$). The eigenstates of the Hamiltonian are calculated by solving the eigenvalue problem

$$\hat{H}_o\psi_i = E_i\psi_i \tag{38}$$

$$\hat{H}_o = -\frac{1}{2}\nabla^2 + V_{SAE}(\mathbf{r}), \tag{39}$$

where ψ_i is an eigenstate and E_i is the corresponding energy. An important detail in determining the bound states is the boundary condition that we impose on the states. We defined the states of the system before as

$$\psi(\mathbf{r},t) = \sum_{lm} \frac{\chi_l(r)}{r} Y_{lm}(\theta,\phi). \tag{40}$$

To find the states of the system, we only need to calculate the radial portion of the wave function. The angular portion is specified by the spherical harmonic functions. To calculate the radial part we write the equation above as

$$r\psi(\mathbf{r},t) = \sum_{lm} \chi_l(r) Y_{lm}(\theta,\phi). \tag{41}$$

This form puts a constraint on the radial function $\chi(r) = 0$ at $r = 0$. This gives us the boundary condition necessary to find a unique solution to the time-independent Schrödinger equation. In our ab-initio method, bound states are calculated using the Krylov-Schur method provided by an algorithm in the SLEPc library [**?**]. The matrix elements for the kinetic energy and SAE potential do not couple states with different orbital quantum numbers and are independent of the magnetic quantum number. This allows the calculations for

eigenstates with different orbital quantum numbers to be carried out independently and the states can be labeled using the principle and orbital quantum numbers. For the basis used in our solution, Eq. 38 can be written as

$$\hat{H}_o \chi_l(r) = E_i \chi_l(r) \tag{42}$$

where $\chi_l(r)$ are the radial functions given in Eq. 6. The calculations for the continuum states can be carried out in a similar manner. However, the finite representation of our wave function on the grid will discretize the energies of the continuum states. With this approach, the continuum states that can be calculated are limited by the size of the grid and the grid spacing used to represent the wave functions. Another approach is to use the shooting method [**?**,**?**] to calculate the continuum states. With the shooting method, a continuum state can be determined for any choice in energy allowing for a preselected range and resolution in the energies of the states that are needed. We implement the shooting method as outlined in [**?**] to calculate the continuum states used in our solution of the TDSE. The shooting method is a valuable technique employed in our numerical solution, allowing us to convert a boundary value problem into an initial value problem. We use $\phi_{kl}(r)$ to denote the continuum radial functions where k and l represent the energy and angular momentum quantum numbers, respectively. The process begins at the boundary point $r_0 = 0$ and proceeds toward the edge of the grid as we propagate the solution. At the boundary point $r_0 = 0$, the value of the wave function is established based on the boundary condition we impose on the radial function, as explained above. More specifically, we set $\phi_{kl}(r_0) = 0$. To initiate the iterative procedure of the shooting method, we assign an arbitrary non-zero value to the wave function at $r_1 = dr$, denoted as $\phi_{kl}(r_1)$. Specifically, we set $\phi_{kl}(r_1)$ to 1. This assumption is valid and provides the correct solution up to a constant factor. Subsequently, we normalize the wave function, which adjusts $\phi_{kl}(r_1)$ to the accurate value. Subsequent points on the grid are computed using the following iterative formula:

$$\phi_{kl}(r_{i+1}) = \phi_{kl}(r_i)\left(dr^2\left[\frac{l(l+1)}{r^2} + 2V(r_i) - 2E\right] + 2\right) - \phi_{kl}(r_{i-1}). \tag{43}$$

Once we have obtained the wave function values using the shooting method, we can normalize the wave function by utilizing the asymptotic solution for the Coulomb potential. The asymptotic solution is given by the Coulomb wave function:

$$\phi_{kl}(r \gg 1) = \sin\left(kr - \frac{l\pi}{2} + \frac{Z}{k}\ln(2kr) + \delta_{kl}\right), \tag{44}$$

where δ_{kl} represents the phase shift calculated in [**?**]. As long as our grid is sufficiently large and the solution obtained through the shooting method matches the Coulomb wave with a phase shift, it is valid to use the asymptotic solution for normalization. The normalization factor for the continuum states is given

by:

$$A_{kl} = \left[\frac{1}{\sqrt{|\phi_{kl}(r)|^2 + \left| \frac{\phi' kl(r)}{(k + \frac{Z}{kr})} \right|^2}} \right]_{r=r_{max}} . \tag{45}$$

By incorporating this factor, we obtain the accurate radial functions for the continuum states. The phase shift is important when utilizing these continuum waves to compute observables and is calculated by matching the phase of our radial function with the asymptotic solution. The phase is given by

$$\delta_{kl} = \left[\arg \left(\frac{i\phi_{kl}(r) + \frac{i\phi'_{kl}(r)}{k + \frac{Z}{kr}}}{(2kr)^{iZ/k}} - kr + \frac{l\pi}{2} \right) \right]_{r=r_{max}} . \tag{46}$$

To find a detailed explanation for the normalization factor and phase equations please refer to [**?**]. To validate our work, we have compared the states obtained using the shooting method with those obtained through Hamiltonian diagonalization and we obtain the same states. The shooting method is applicable to atomic systems with spherically symmetric potentials, and we have employed it for the ionization processes we have studied in the work presented in this thesis. From a computational standpoint, the shooting method is favored over diagonalization. This preference arises due to the extensive time and memory resources required for diagonalizing large matrices.

6.7 Time propagation

The Crank-Nicolson method is employed to propagate the wave function as a function of time. By utilizing this method, the wave function undergoes a unitary time evolution, guaranteeing the preservation of its norm throughout the propagation process. The total Hamiltonian is employed for the propagation, and each subsequent time step is calculated accordingly. The propagation step is given by

$$\psi(\mathbf{r}, t + \Delta t) \approx e^{-i\hat{H}\Delta t} \psi(\mathbf{r}, t), \tag{47}$$

where

$$e^{-i\hat{H}\Delta t} \approx \frac{1 - i\frac{\Delta}{2}\hat{H}}{1 + i\frac{\Delta}{2}\hat{H}}. \tag{48}$$

Using Equations 47 and 48 the second order Crank-Nicolson scheme for the time propagation can be written as

$$\left(1 + i\frac{\Delta}{2}\hat{H}\right) \psi(\mathbf{r}, t + \Delta t) = \left(1 - i\frac{\Delta}{2}\hat{H}\right) \psi(\mathbf{r}, t). \tag{49}$$

The selection rules outlined in section 6.4 result in sparse matrices when applying the Crank-Nicolson method to the system of equations. These sparse matrices enable the utilization of iterative algorithms, facilitating efficient time

propagation. To achieve this, we employ the PETSc library [**?**, **?**] and its implementation of the Generalized Minimal Residual Method (GMRES) for solving linear equations during time propagation. The PETSc library simplifies the parallelization of the Crank-Nicolson method, allowing our calculations to be executed on multiple cores with a performance that scales linearly.

During time propagation, a portion of the wave function might reach the end of the grid allocated to represent the wave function. This results in the reflection of outgoing wave packets that reach the end of the grid. Reflections from the edge cause nonphysical interference effects, leading to numerical errors in our solution. To remove the reflections, we implement the exterior complex scaling method [**?**] on the edge of the grid. The ECS method rotates a portion of the grid into the complex plane leading to an exponential decay of the wave function at the edge of the grid. We implement the ECS using the procedure outlined in [**?**, **?**].

6.8 Observables

The time-propagated wave function is used to calculate all the relevant observables for our study. The value of an observable is determined by taking the expectation value of the corresponding operator with the time-propagated wave function. For operator $\hat{O}$ the expectation value is given by

$$Observable = \left| \left\langle \Psi \left| \hat{O} \right| \Psi \right\rangle \right|^2, \tag{50}$$

where Ψ is the time-propagated wave function. The observables studied in this thesis are the population of bound states, ionization probability, and photo-electron spectrum. The population for a given state is calculated by projecting the time-propagated wave function on the corresponding bound or continuum state. The population in the bound states is given by

$$P_{\phi_n} = \left| \langle \phi_n | \Psi \rangle \right|^2, \tag{51}$$

where ϕ_n is the n^{th} bound state. Since the Crank-Nicolson method preserves the norm of the wave function, the ionization probability can be calculated by subtracting the population in the bound states from unity as

$$P_{ionization} = 1 - \sum_n \left| \langle \phi_n | \Psi \rangle \right|^2. \tag{52}$$

The photo-electron spectrum can be obtained from the time-propagated wave function as

$$F(k, \phi, \theta) = \frac{1}{k^2} \left| \sum_{l,m} \left[\int e^{-i\delta_{kl}} (i)^l \phi_{kl}(r)^* \psi(r,t)\, dx \right] Y^*_{l,m}(\phi, \theta) \right|^2 \tag{53}$$

where $Y^*_{l,m}(\phi, \theta)$ are the spherical harmonics, δ_{kl} is the phase shift, and $\phi_{kl}(r)$ is a continuum state with momentum k. The methods for calculating the continuum states and phase shift are outlined in section 6.6.

7 Laser pulses

In both the ab-initio solution and QTMC simulations, we simulate the interaction between atoms and laser pulses. In this section, we explain how we define the laser pulses that we use in our simulations. Laser pulses release light in short bursts lasting from attoseconds to milliseconds. As the pulses are time-limited, they contain photons in a frequency range around the central frequency. Defining the laser field can be done either by using its electric field or vector potential. For pulsed lasers with an envelope shape, defining the laser pulse through its electric field results in a non-zero vector potential. To ensure that the potential disappears at the end of the pulse, as stated in [**?**], we first define the vector potential and then derive the electric field from it. The vector potential is defined as

$$\mathbf{A}(t) = \frac{A_o}{\sqrt{1+\epsilon^2}} \left[\cos(\omega_A t + \phi)\hat{x} + \epsilon \sin(\omega_A t + \phi)\hat{y}\right] f(t) \tag{54}$$

where A_o is the electric potential amplitude, ω_A is the central frequency and ϕ is the carrier-envelope phase. The laser field is polarized in the $x-y$ plane and propagates in the $\hat{z}$ direction. ϵ is the ellipticity of the field that determines the polarization state of the laser light. The intensity of laser pulses is connected to the amplitude of the electric potential via the equation $A_o = \sqrt{\frac{I}{I_o \omega}}$, where $I_o = 3.51 \times 10^{16}$ W/cm^2. The pulse envelope function $f(t)$ governs the pulse shape, and there are various envelope functions available. Two commonly used envelope functions are provided as examples in Eq. 55. An example of a sin-squared laser pulse is depicted in Fig. 2 where we show both the field (blue) and the envelope (red) of the pulse.

$$f(t) = \begin{cases} \sin^2(\frac{\pi t}{\tau}), & \text{sin-squared envelope} \\ \exp\left(-\ln(2)\ (\frac{2t}{\tau})^2\right), & \text{Gaussian envelope} \end{cases} \tag{55}$$

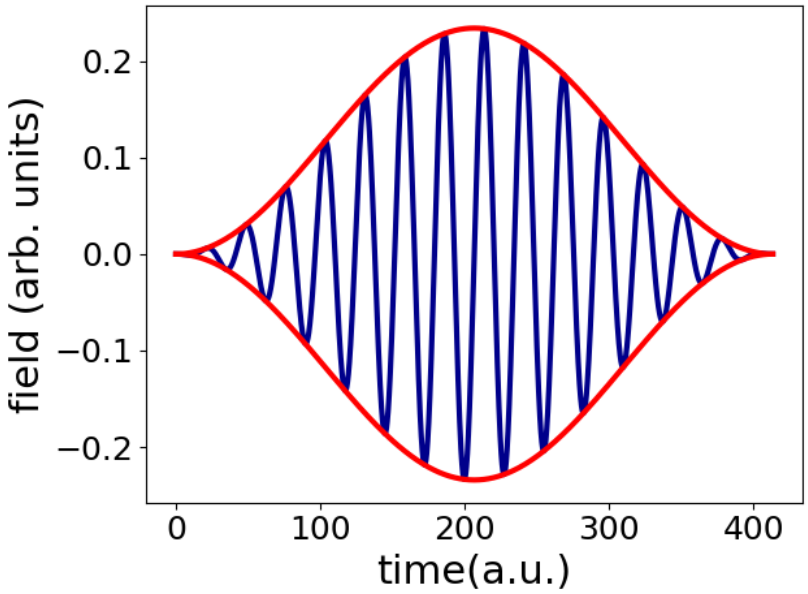

Figure 2: Temporal profile of a laser pulse with 200 nm wavelength, 1×10^{14} W/cm^2 intensity, and 15 cycles. The red line depicts the envelope function, while the blue line represents the electric field.

The electric field can be calculated from the vector potential using the relation

$$E(t) = -\frac{1}{c}\frac{\partial}{\partial t}A(t). \tag{56}$$

For a simple linearly polarized laser pulse such as

$$\mathbf{A}(t) = \frac{A_o}{\sqrt{1+\epsilon^2}}\cos(\omega_A t + \phi)f(t), \tag{57}$$

the electric field is given by

$$E(t) = -\frac{1}{c}\frac{\partial}{\partial t}A(t) = E_o \sin(\omega_A t + \phi)f(t) - \frac{E_o}{\omega_A}\cos(\omega_A t + \phi)\frac{\partial f(t)}{\partial t}. \tag{58}$$

where $E_o = \omega_A A_o$. A consequence of defining the electric field in this manner is that the central frequencies of the electric field and vector potential are not the same [**?**]. This is due to the second term in Eq. 58 leading to a frequency shift defined by $|\omega_E - \omega_A|$. As shown in [**?**], the ratio of the frequencies is given by

$$\frac{\omega_E}{\omega_A} \approx \frac{1+\sqrt{1+4(\pi N)^{-2}}}{2}, \quad \text{where} \quad N = \frac{\omega_A}{\pi}\sqrt{\frac{\int_{-\infty}^{\infty}(t-t_o)^2 f(t)dt}{\int_{-\infty}^{\infty} f(t)dt}}. \tag{59}$$

In the above equation N is the number of cycles that are with one standard deviation of the peak of the pulse and t_o is given by

$$t_o = \frac{\int_{-\infty}^{\infty} t f(t) dt}{\int_{-\infty}^{\infty} f(t) dt}. \tag{60}$$

The ratio of the frequencies given by Eq. 59 depends on the pulse shape and number of cycles of the pulse. It is, however, independent of other laser parameters. The frequency shift becomes negligible as the number of cycles of the pulse increases. To properly model the laser coupling interaction as described in section 6, one needs to use the corrected frequency for the vector potential. Further information about the frequency shift and its effects on the solution to the TDSE can be found in [**?**].